Title

Three-dimensional adiabatic inversion recovery prepared ultrashort echo time cones (3D IR-UTE-Cones) imaging of cortical bone in the hip

Authors

Nazaran, Amin
Carl, Michael
Ma, Yajun
et al.

Publication Date

2017-12-01

DOI

10.1016/j.mri.2017.07.012

Magnetic Resonance Imaging 44 (2017) 60–64

Contents lists available at ScienceDirect

Magnetic Resonance Imaging

journal homepage: www.mrijournal.com

Technical note

Three-dimensional adiabatic inversion recovery prepared ultrashort echo time cones (3D IR-UTE-Cones) imaging of cortical bone in the hip

Amin Nazaran [a,*], Michael Carl [b], Yajun Ma [a], Saeed Jerban [a], Yanchun Zhu [a], Xing Lu [a], Jiang Du [a], Eric Y. Chang [c,a]

[a] Department of Radiology, University of California, San Diego, CA, United States
[b] Applied Science Lab, GE Healthcare, San Diego, CA, United States
[c] Radiology Service, VA San Diego Healthcare System, San Diego, CA, United States

ARTICLE INFO

Article history:
Received 19 May 2017
Accepted 13 July 2017

Keywords:
Cortical bone
Hip
UTE
Cones
Adiabatic inversion recovery
T_2^*

ABSTRACT

Purpose: We present three-dimensional adiabatic inversion recovery prepared ultrashort echo time Cones (3D IR-UTE-Cones) imaging of cortical bone in the hip of healthy volunteers using a clinical 3T scanner.
Methods: A 3D IR-UTE-Cones sequence, based on a short pulse excitation followed by a 3D Cones trajectory, with a nominal TE of 32 μs, was employed for high contrast morphological imaging of cortical bone in the hip of heathy volunteers. Signals from soft tissues such as muscle and marrow fat were suppressed via adiabatic inversion and signal nulling. T_2^* value of the cortical bone was also calculated based on 3D IR-UTE-Cones acquisitions with a series of TEs ranging from 0.032 to 0.8 ms. A total of four healthy volunteers were recruited for this study. Average T_2^* values and the standard deviation for four regions of interests (ROIs) at the greater trochanter, the femoral neck, the femoral head and the lesser trochanter were calculated.
Results: The 3D IR-UTE-Cones sequence provided efficient suppression of soft tissues with excellent image contrast for cortical bone visualization in all volunteer hips. Exponential single component decay was observed for all ROIs, with averaged T_2^* values ranging from 0.33 to 0.45 ms, largely consistent with previously reported T_2^* values of cortical bone in the tibial midshaft.
Conclusions: The 3D IR-UTE-Cones sequence allows in vivo volumetric imaging and quantitative T_2^* measurement of cortical bone in the hip using a clinical 3T scanner.

1. Introduction

The femoroacetabular joint is a key skeletal element that provides a great deal of mobility and stability. Large loads are exerted on the hip during daily activities, such as walking or running, where forces can exceed five times body weight [1]. Unfortunately fractures can occur, and hip fractures are among the most frequent and devastating of all fractures, particularly in women and the elderly [2,3]. The mortality rate within the first year after a hip fracture may reach up to 30%, which is considerably higher than the mortality rate of breast cancer [4–10].

Hip fractures occur where the applied load is higher than the bone strength [11]. Cortical bone is an important contributor to overall bone strength [12]. Cortical bone strength and toughness, or simply the fracture resistance, can be decreased dramatically by microstructural changes such as reductions in thickness and density, or increases in porosity [13,14]. In vivo evaluation of cortical bone microstructure has been of great interest in both the orthopedic and radiologic communities [12,15,16]. Many research teams have attempted to quantify bone microstructure and assess the predictive value of various measures in determining fracture risk [17,18].

Magnetic resonance (MR) imaging is a non-invasive imaging modality that can be used to evaluate cortical bone. However, the current, clinically available MR sequences are not able to image cortical bone because the signal from the cortical bone decays rapidly. Therefore, the cortical bone in the clinical images usually appears black (pure signal void). Ultrashort echo time (UTE) techniques can acquire the rapidly decaying MR signal from cortical bone. In recent years, a variety of UTE techniques have been developed to image cortical bone [19–24]. Almost all the UTE techniques have focused on cortical bone in the tibial midshaft, with a few examples showing success in imaging the femur and the forearm [25]. Direct MR imaging of cortical bone in the hip with inversion recovery UTE (IR-UTE) technique has not yet been performed.

MR imaging of the cortical bone in the hip has traditionally been fraught with challenges. The main technical difficulties in this area are: 1) the thin cortex, 2) inefficient coils, 3) requirement for robust suppression of surrounding soft tissues to generate high contrast, and 4) long scan time. Also, the thin cortex requires high resolution, which in turn leads to limited signal-to-noise ratio (SNR). The SNR requirement can be moderated by utilizing efficient coils contoured for the

* Corresponding author at: University of California at San Diego, Department of Radiology, La Jolla, CA 92093, United States.
E-mail address: anazaran@ucsd.edu (A. Nazaran).

http://dx.doi.org/10.1016/j.mri.2017.07.012
0730-725X/

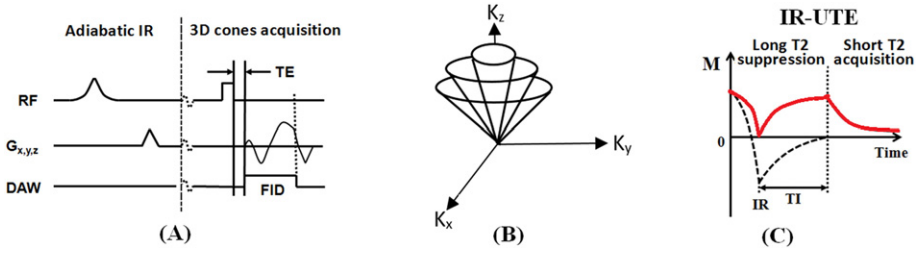

Fig. 1. The 3D UTE-Cones sequence employs a short rectangular pulse for signal excitation, followed by a 3D Cones trajectory (B) to allow time-efficient sampling with a minimal TE of 32 μs. The 3D UTE-Cones sequence combined with an adiabatic inversion recovery preparation pulse (3D IR-UTE-Cones) can invert and null the signal from long T_2^* components, including fat and muscle, allowing the cortical bone to be selectively imaged (C). In (C), the dashed curve line and the red solid line represent the long T_2^* components and the short T_2^* components, respectively. The dotted line illustrates that after time TI the signal from the long T_2^* components is nulled (reaching zero) while a significant amount of signal from the short T_2^* components remains.

structure of interest, however, there are no commercially available coils for dedicated hip imaging. In addition, to create high contrast images, cortical bone signal must be preserved while undesired components are suppressed. This includes fat in the marrow and extramedullary locations as well as surrounding long T_2 structures such as muscle.

In this study, we report the use of three-dimensional adiabatic inversion recovery prepared UTE with Cones sampling (3D IR-UTE-Cones) to directly image and quantify cortical bone in the hip in vivo at 3 T.

2. Methods

2.1. Pulse sequence

The 3D UTE-Cones sequence is shown in Fig. 1A. The 3D UTE-Cones sequence employs a hard RF pulse for non-selective excitation, and center-out 3D spiral trajectories for k-space sampling [26], as shown in Fig. 1B. It also employs short readout times, which in combination with the centric trajectory, allows for signal acquisition from the rapidly decaying tissue components. The 3D UTE-Cones sequence is more time-efficient than radial trajectories in covering 3D k-space [26]. Also, the 3D UTE-Cones sequence resolves the sensitivity of the 2D UTE sequences to eddy currents by employing a hard RF pulse instead of a half RF pulse for signal excitation. Moreover, the 3D UTE-Cones sequence allows for anisotropic fields of view (FOVs) and spatial resolution (higher in-plane resolution with thicker slices), resulting in vastly reduced scan times. By using the 3D UTE-Cones sequence, 3D volumetric UTE imaging can be obtained in an SNR efficient way.

When followed by an adiabatic inversion recovery preparation pulse, the 3D UTE-Cones sequence can be utilized to acquire signal from cortical bone with high contrast [27,28]. This is done by inverting the longitudinal magnetization of the long T_2 signal components (i.e., muscle and bone marrow fat) while saturating the signal from cortical bone [27–31]. The Cones acquisition starts after an inversion time (TI) delay, which is used to null the long T_2^* components while permitting detection of recovered cortical bone signal (Fig. 1C).

2.2. T_2^* measurement with 3D IR-UTE-Cones

The steady-state 3D IR-UTE-Cones signal can be calculated as follows:

$$M_{xy}^{IR}(TI, TE) = M_0^{IR}\, e^{-\frac{TE}{T_2}} + \text{noise}, \quad (1)$$

Eq. (1) describes that T_2^* of cortical bone can be measured by mono exponential fitting of the acquired IR-UTE images at different TEs. It should be noted that TR/TI combination should be able to null the signal from the long T_2 components in the bone marrow and muscle.

2.3. MRI protocol

The 3D IR-UTE-Cones sequence was implemented on a 3 T scanner (Signa HDx, GE Healthcare, Milwaukee, WI) [27]. The sequence has a minimal TE of 32 μs and allows anisotropic field of view and spatial resolution for fast volumetric imaging. An adiabatic inversion pulse (duration = 8.64 ms) was used for robust inversion and suppression of the longitudinal magnetizations of long T2 water and fat. Four healthy volunteers (28, 31, 34, and 43 years old, male) were scanned by using a torso phased-array coil. The following scan parameters were used: TR = 116.7 ms, TI = 50 ms, four TEs (0.032, 0.2, 0.4, and 0.8 ms), BW = 250 kHz, FOV = 340 × 340 mm^2, slice thickness = 3 mm, matrix = 128 × 128, flip angle = 18°, acquired voxel size = 2.6 × 2.6 × 3 mm^3, and scan time = 4.5 min for each dataset. T_2^* was quantified with a single-component decay fitting of the multi-echo 3D IR-UTE-Cones images.

2.4. Data analysis

The code for the analysis was written in MATLAB (The MathWorks, Massachusetts) and was executed on the DICOM images obtained by the aforementioned protocols in the experimental setup section. The program allowed for the delineation of regions of interest (ROIs) on

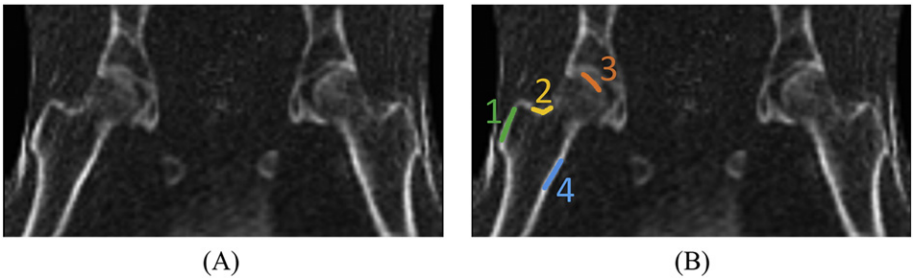

Fig. 2. (A) The 3D IR-UTE-Cones sequence provides excellent image contrast for cortical bone in the hip obtained with TR = 116.7 ms, TI = 50 ms and TE = 0.032 ms for a healthy volunteer (34-year-old man); (B) Four representative ROIs are defined for T_2^* analysis, including the greater trochanter (ROI1), the lateral aspect of the femoral neck (ROI2), the femoral head (ROI3), and the lesser trochanter (ROI4). The approximate locations of the selected ROIs are shown in the figure with different colors.

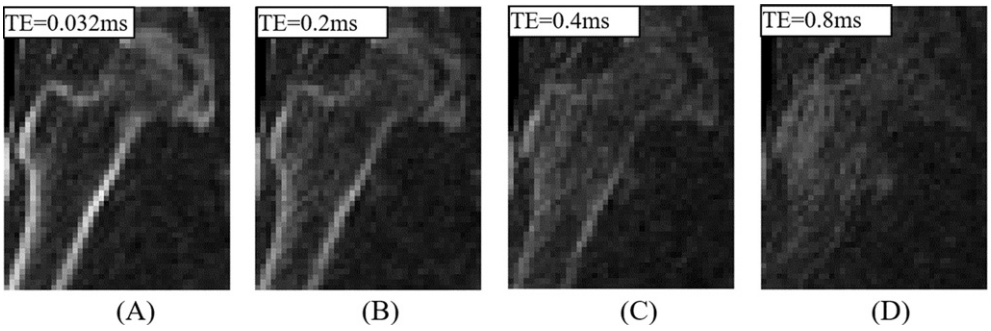

Fig. 3. 3D IR-UTE-Cones images of the right hip in a healthy volunteer at TEs = 0.032 ms, 0.2 ms, 0.4 ms and 0.8 ms from left to right, respectively. Excellent contrast for the cortical bone in the hip can be achieved.

the UTE images. Four ROIs were drawn in the proximal femur for T_2^* analysis. As shown in Fig. 2, ROIs included the greater trochanter (ROI1), the lateral aspect of the femoral neck (ROI2), the femoral head (ROI3), and the lesser trochanter (ROI4). The average intensity of voxels within the ROIs was used for subsequent curve fitting. In addition, T_2^* of the cortical bone were calculated using Eq. (1).

3. Results

Fig. 2 shows a representative image of the hip of a 34-year-old healthy volunteer imaged with the 3D IR-UTE-Cones sequence. Cortical bone in the greater trochanter, the femoral neck, and the femoral head, as well as lesser trochanter is depicted with excellent image contrast. Muscle and marrow fat about the hip, which typically have far higher signal than that of cortical bone, were efficiently suppressed by the adiabatic inversion pulse. SNR for cortical bone in the femoral head is relatively low due to the thin structure and limited coil sensitivity from the clinical torso phased array coil.

Cortical bone in the hip at four different TEs of 0.032, 0.2, 0.4 and 0.8 ms is shown in Fig. 3. As can be seen, excellent contrast can be achieved by using the 3D IR-UTE-Cones sequence with rapid decay of signal. Fig. 4 shows representative signal decay curves for the greater trochanter, the femoral neck, the femoral head, and the lesser trochanter in a 34-year-old male volunteer. Excellent single-component exponential decay was observed for all the ROIs, with a short T_2^* of 0.41 ± 0.11 ms for the greater trochanter, 0.33 ± 0.08 ms for the femoral neck, 0.34 ± 0.05 ms for the femoral head, and 0.33 ± 0.04 ms for the lesser trochanter.

Table 1 summarizes the mean and standard deviation for T_2^* values for the greater trochanter, the femoral neck, the femoral head, and the lesser trochanter, respectively, between the four volunteers. The average T_2^* values ranged from 0.33 to 0.45 ms, and were largely consistent with previously reported T_2^* values of bound water in the tibial midshaft.

4. Discussion

In this study, a direct MR-based imaging technique, based on IR-UTE technique, for cortical bone in the hip was reported for the first time in vivo. Although direct imaging of cortical bone has previously been presented at different locations such as the midshaft of the tibia [28,32–34], direct imaging of the hip is considered of higher clinical significance since fractures at this location are more devastating [3]. In addition, imaging at this location is considered more technically challenging.

Preliminary results from this study have shown that the cortical bone in the hip can be imaged using the 3D IR-UTE-Cones sequence (Fig. 3). The adiabatic inversion pulse provides robust suppression of

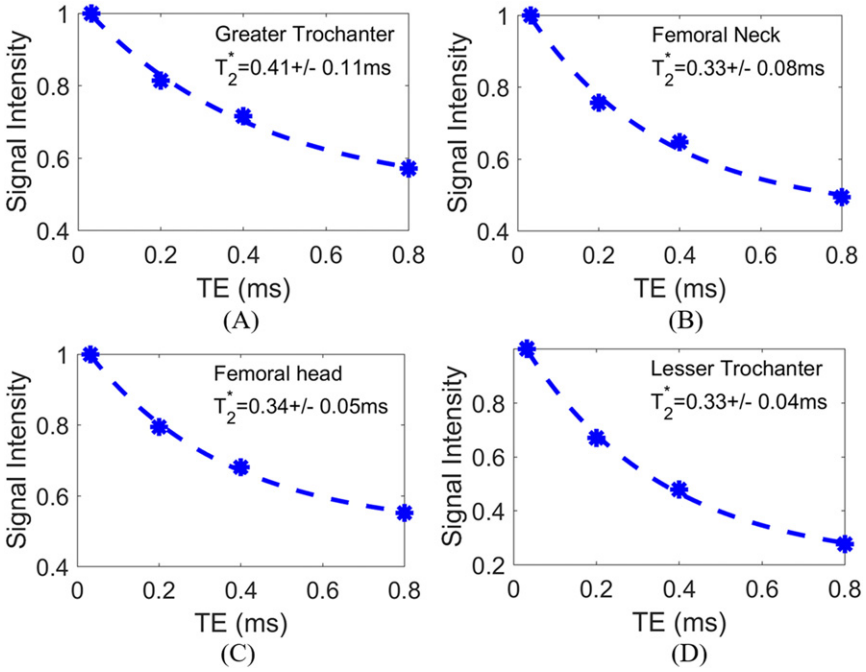

Fig. 4. Representative T_2^* curves for ROIs 1 through 4 at TEs = 0.032 ms, 0.2 ms, 0.4 ms and 0.8 ms. The star points and the dashed lines in the figures represent the normalized average signal in the ROI and the fitted curves, respectively. As TE values increase, the amount of signal from the cortical bone decreases.

Table 1
Average T_2^* values (ms) and the standard deviation for four healthy volunteers. The T_2^* values were calculated at the four ROIs on the right and left side for each subject. ROIs 1 through 4 were defined at the greater trochanter (ROI1), the femoral neck (ROI2), the femoral head (ROI3), and the lesser trochanter (ROI4), respectively.

	Cortical bone in different sites of the hip			
	Greater trochanter	Femoral neck	Femoral head	Lesser trochanter
T_2^* in ms (mean ± std)	0.40 ± 0.05	0.38 ± 0.04	0.37 ± 0.04	0.38 ± 0.03

long T_2 signal. Despite long T_2 muscle and fat containing distinct T_1 values, both can be adequately suppressed with the single IR pulse, resulting in a high contrast, selective imaging technique for cortical bone. T_2^* can then be estimated via single-component fitting of the 3D IR-UTE-Cones acquisitions with a series of TEs (Fig. 4).

Using the 3D IR-UTE-Cones technique, cortical bone may be visualized with high contrast and T_2^* may be quantified, providing a single method to measure thickness and estimate porosity, respectively. Cortical bone thickness and porosity are both considered key elements for fracture risk [12,15–18]. Specifically, cortical bone thinning and increasing porosity are important features for fracture initiation and propagation [15,16]. Different image processing techniques [35,36] can be used for accurate thickness calculation and to pinpoint thin and weak cortical bone locations.

The UTE and IR-UTE sequences can potentially evaluate cortical porosity (pore water content) and organic matrix (bound water content) in the hip [27,33,37–41]. Previous studies employing the UTE sequence have shown that both bound water (short T_2^* component) and pore water (long T_2^* component) in cortical bone can be quantified using a bi-component T_2^* analysis technique [18,25–28]. Moreover, T_2^* decay time for bound water in cortical bone can be measured with the IR-UTE technique by suppressing the signal from the pore water and then using a single component analysis of the remaining signal [27,29,38]. A single component decay pattern of the cortical bone in the hip suggests that the 3D IR-UTE-Cones signal is likely from bound water.

One limitation of the 3D IR-UTE-Cones technique is that it requires an adiabatic inversion pulse, which can increase the specific absorption ratio (SAR). This problem can be moderated by using lower flip angles at a cost of sub-optimal contrast, or longer TR at a cost of longer scan time. Another limitation is that UTE with an inversion pulse requires a wide spectral profile to cover both water and fat peaks for robust inversion. Also, the 3D IR-UTE-Cones sequence requires more time to cover k-space compared to 2D UTE imaging techniques. However, the 3D IR-UTE-Cones sequence is less prone to partial volume effects.

Further optimization of the imaging protocol, including in-plane resolution, slice thickness and scan time will be performed in future studies. In addition to further optimization techniques, 3D IR-UTE-Cones sequence should be employed in multiple cohorts. These future studies will help in defining the limitations and thresholds for direct MR imaging of cortical bone.

5. Conclusion

Our pilot study has demonstrated the feasibility of selective MR imaging of cortical bone in the hip using the 3D IR-UTE-Cones technique. Long-T_2 species (e.g., fat in bone marrow and muscle) were robustly suppressed, providing high image contrast for the cortical bone in clinically compatible imaging times.

Acknowledgments

The authors acknowledge grant support from GE Healthcare, the National Institutes of Health [grant numbers: 1R01 AR062581-01A1, 1R01 AR068987-01] and the VA Clinical Science Research and Development Service [Merit Award I01CX001388].

Conflicts of interest

None.

References

[1] van den Bogert AJ, Read L, Nigg BM. An analysis of hip joint loading during walking, running, and skiing. Med Sci Sport Exerc 1999;31:131–42. http://dx.doi.org/10.1097/00005768-199901000-00021.
[2] Cummings SR, Nevitt MC, Browner WS, Stone K, Fox KM, Ensrud KE, et al. Risk factors for hip fracture in white women. Study of osteoporotic fractures research group. N Engl J Med 1995;332:767–73.
[3] Panula J, Pihlajamaki H, Mattila VM, Jaatinen P, Vahlberg T, Aarnio P, et al. Mortality and cause of death in hip fracture patients aged 65 or older: a population-based study. BMC Musculoskelet Disord 2011;12:105.
[4] Ward RJ, Weissman BN, Kransdorf MJ, Adler R, Appel M, Bancroft LW, et al. ACR appropriateness criteria acute hip pain—suspected fracture. J Am Coll Radiol 2013:1–7. http://dx.doi.org/10.1016/j.jacr.2013.10.023.
[5] Brauer CA, Coca-Perraillon M, Cutler DM, Rosen AB. Incidence and mortality of hip fractures in the United States. JAMA 2009;302:1573–9.
[6] Currie S, Hadjivassiliou M, Craven IJ, Wilkinson ID, Griffiths PD, Hoggard N. Magnetic resonance imaging biomarkers in patients with progressive ataxia: current status and future direction. Cerebellum 2012;12:245–66. http://dx.doi.org/10.1007/s12311-012-0405-3.
[7] Rehman H, Clement RGE, Perks F, White TO. Imaging of occult hip fractures: CT or MRI? Injury 2016. http://dx.doi.org/10.1016/j.injury.2016.02.020.
[8] L PH, S EA. Factors influencing mortality in hip fractures. Am J Surg 1964;108:645–8.
[9] Kenzora JE, McCarthy RE, Lowell JD, Sledge CB. Hip fracture mortality. Relation to age, treatment, preoperative illness, time of surgery, and complications. Clin Orthop Relat Res 1984:45–56. http://dx.doi.org/10.1097/00003086-198406000-00008.
[10] L AR, K DB, L P, C C. Clinical outcomes and treatment of hip fractures. Am J Med 1997;103:51S–64S.
[11] Johannesdottir F, Turmezei T, Poole KES. Cortical bone assessed with clinical computed tomography at the proximal femur. J Bone Miner Res 2014;29:771–83. http://dx.doi.org/10.1002/jbmr.2199.
[12] Johannesdottir F, Poole KES, Reeve J, Siggeirsdottir K, Aspelund T, Mogensen B, et al. Distribution of cortical bone in the femoral neck and hip fracture: a prospective case-control analysis of 143 incident hip fractures; the AGES-REYKJAVIK study. Bone 2011;48:1268–76. http://dx.doi.org/10.1016/j.bone.2011.03.776.
[13] Tarantino U, Rao C, Tempesta V, Gasbarra E, Feola M. Hip fractures in the elderly: the role of cortical bone. Injury 2016. http://dx.doi.org/10.1016/j.injury.2016.07.058.
[14] Bae WC, Chen PC, Chung CB, Masuda K, D'Lima D, Du J. Quantitative ultrashort echo time (UTE) MRI of human cortical bone: correlation with porosity and biomechanical properties. J Bone Miner Res 2012;27:848–57. http://dx.doi.org/10.1002/jbmr.1535.
[15] Poole KES, Treece GM, Mayhew PM, Vaculík J, Dungl P, Horák M, et al. Cortical thickness mapping to identify focal osteoporosis in patients with hip fracture. PLoS One 2012;7. http://dx.doi.org/10.1371/journal.pone.0038466.
[16] Yang L, Udall WJM, McCloskey EV, Eastell R. Distribution of bone density and cortical thickness in the proximal femur and their association with hip fracture in postmenopausal women: a quantitative computed tomography study. Osteoporos Int 2014;25:251–63. http://dx.doi.org/10.1007/s00198-013-2401-y.
[17] Treece GM, Gee AH, Tonkin C, Ewing SK, Cawthon PM, Black DM, et al. Predicting hip fracture type with cortical bone mapping (CBM) in the osteoporotic fractures in men (MrOS) study. J Bone Miner Res 2015;30:2067–77. http://dx.doi.org/10.1002/jbmr.2552.
[18] Liebl H, Garcia EG, Holzner F, Noel PB, Burgkart R, Rummeny EJ, et al. In-vivo assessment of femoral bone strength using finite element analysis (FEA) based on routine MDCT imaging: a preliminary study on patients with vertebral fractures. PLoS One 2015;10. http://dx.doi.org/10.1371/journal.pone.0116907.
[19] Wu Y, Ackerman JL, Chesler DA, Graham L, Wang Y, Glimcher MJ. Density of organic matrix of native mineralized bone measured by water- and fat-suppressed proton projection MRI. Magn Reson Med 2003;50:59–68. http://dx.doi.org/10.1002/mrm.10512.
[20] Du J, Hamilton G, Takahashi A, Bydder M, Chung CB. Ultrashort echo time spectroscopic imaging (UTESI) of cortical bone. Magn Reson Med 2007;58:1001–9. http://dx.doi.org/10.1002/mrm.21397.
[21] Techawiboonwong A, Song HK, Leonard MB, Wehrli FW. Cortical bone water: in vivo quantification with ultrashort echo-time MR imaging. Radiology 2008;248:824–33. http://dx.doi.org/10.1148/radiol.2482071995.
[22] Reichert IL, Robson MD, Gatehouse PD, He T, Chappell KE, Holmes J, et al. Magnetic resonance imaging of cortical bone with ultrashort TE pulse sequences. Magn Reson Imaging 2005;23:611–8. http://dx.doi.org/10.1016/j.mri.2005.02.017.
[23] Seifert AC, Li C, Wehrli SL, Wehrli FW. A surrogate measure of cortical bone matrix density by long T2-suppressed MRI. J Bone Miner Res 2015;30:2229–38. http://dx.doi.org/10.1002/jbmr.2580.
[24] Abbasi-Rad S, Saligheh Rad H. Quantification of human cortical bone bound and free water in vivo with ultrashort echo time MR imaging: a model-based approach. Radiology 2017;0:160780. http://dx.doi.org/10.1148/radiol.2016160780.
[25] Johnson EM, Vyas U, Ghanouni P, Pauly KB, Pauly JM. Improved cortical bone specificity in UTE MR imaging. Magn Reson Med 2016. http://dx.doi.org/10.1002/mrm.26160.
[26] Gurney PT, Hargreaves BA, Nishimura DG. Design and analysis of a practical 3D cones trajectory. Magn Reson Med 2006;55:575–82. http://dx.doi.org/10.1002/mrm.20796.

[27] Carl M, Bydder GM, Du J. UTE imaging with simultaneous water and fat signal suppression using a time-efficient multispoke inversion recovery pulse sequence. Magn Reson Med 2016;76:577–82. http://dx.doi.org/10.1002/mrm.25823.
[28] Chen J, Chang EY, Carl M, Ma Y, Shao H, Chen B, et al. Measurement of bound and pore water T_1 relaxation times in cortical bone using three-dimensional ultrashort echo time cones sequences. Magn Reson Med 2016;0:1–10. http://dx.doi.org/10.1002/mrm.26292.
[29] Li S, Ma L, Chang EY, Shao H, Chen J, Chung CB, et al. Effects of inversion time on inversion recovery prepared ultrashort echo time (IR-UTE) imaging of bound and pore water in cortical bone. NMR Biomed 2015;28:70–8. http://dx.doi.org/10.1002/nbm.3228.
[30] Horch RA, Gochberg DF, Nyman JS, Does MD. Clinically compatible MRI strategies for discriminating bound and pore water in cortical bone. Magn Reson Med 2012;68:1774–84. http://dx.doi.org/10.1002/mrm.24186.
[31] Du J, Carl M, Bydder M, Takahashi A, Chung CB, Bydder GM. Qualitative and quantitative ultrashort echo time (UTE) imaging of cortical bone. J Magn Reson 2010;207:304–11. http://dx.doi.org/10.1016/j.jmr.2010.09.013.
[32] Manhard MK, Harkins KD, Gochberg DF, Nyman JS, Does MD. 30-Second Bound and Pore Water Concentration Mapping of Cortical Bone Using 2D UTE With, 0; 2017. http://dx.doi.org/10.1002/mrm.26605.
[33] Manhard MK, Horch RA, Gochberg DF, Nyman JS, Does MD. In vivo quantitative MR imaging of bound and pore water in cortical bone. Radiology 2015;277:221–9. http://dx.doi.org/10.1148/radiol.2015140336.
[34] Chen J, Grogan SP, Shao H, D'Lima D, Bydder GM, Wu Z, et al. Evaluation of bound and pore water in cortical bone using ultrashort-TE MRI. NMR Biomed 2015;28:1754–62. http://dx.doi.org/10.1002/nbm.3436.
[35] Jerban S, Elkoun S. Novel linear intercept method for characterizing micropores and grains in calcium phosphate bone substitutes. Mater Charact 2016;119:216–24. http://dx.doi.org/10.1016/j.matchar.2016.08.008.
[36] Hildebrand T, Rüegsegger P. A new method for the model-independent assessment of thickness in three-dimensional images. J Microsc 1997;185:67–75. http://dx.doi.org/10.1046/j.1365-2818.1997.1340694.x.
[37] Rajapakse CS, Bashoor-Zadeh M, Li C, Sun W, Wright AC, Wehrli FW. Volumetric cortical bone porosity assessment with MR imaging: validation and clinical feasibility. Radiology 2015;276:526–35. http://dx.doi.org/10.1148/radiol.15141850.
[38] Du J, Hermida JC, Diaz E, Corbeil J, Znamirowski R, D'Lima DD, et al. Assessment of cortical bone with clinical and ultrashort echo time sequences. Magn Reson Med 2013;70:697–704. http://dx.doi.org/10.1002/mrm.24497.
[39] Rad HS, Lam SCB, Magland JF, Ong H, Li C, Song HK, et al. Quantifying cortical bone water in vivo by three-dimensional ultra-short echo-time MRI. NMR Biomed 2011;24:855–64. http://dx.doi.org/10.1002/nbm.1631.
[40] Li C, Seifert AC, Rad HS, Bhagat Ya, Rajapakse CS, Sun W, et al. Cortical bone water concentration: dependence of MR imaging measures on age and pore volume fraction. Radiology 2014;272:796–806. http://dx.doi.org/10.1148/radiol.14132585.
[41] Du J, Diaz E, Carl M, Bae W, Chung CB, Bydder GM. Ultrashort echo time imaging with bicomponent analysis. Magn Reson Med 2012;67:645–9. http://dx.doi.org/10.1002/mrm.23047.